Basics of Scanning Electrochemical Microscope and its Application in Characterizations of Lithium-Ion Batteries: A Brief Review

Basics of the Scanning Electrochemical Microscope and its Application in Characterization of Lithium-Ion Batteries: A Brief Review

Rong He,[1] Larissa Zhou,[2] Robert Tenent,[3,4,][*] and Meng Zhou[1,][*]

[1]Department of Chemical and Materials Engineering, New Mexico State University, New Mexico 88003, United States. *E-mail: mzhou@nmsu.edu*

[2]Wastach Academy, Mt Pleasant, UT 84647, United States.

[3]National Renewable Energy Laboratory, Golden, CO 80401, United States. *E-mail: robert.tenent@nrel.gov*

[4]Renewable and Sustainable Energy Institute, University of Colorado, Boulder, CO 80309, United States.

Abstract

The scanning electrochemical microscope (SECM) can directly monitor electrochemical processes at interfaces of electrodes and electrolytes and has been used as an analytical tool for lithium-ion battery (LIB) study. Through SECM, we can visualize the electrochemical reactivities of active species in LIBs in-situ during cycling. This review begins with introducing SECM-based LIB research and then summarizes the working mechanism and operating modes of the technique as well as combinations of SECM with other techniques for LIB study. We review results with focus on the interfacial properties, surface reactions and electrochemical activity of different electrode materials for LIBs. The investigations of battery degradation, kinetic parameters and electrolyte swelling by SECM are also discussed. Finally, the current limitations and perspectives are also described regarding future developments.

Keywords: Scanning electrochemical microscope, lithium-ion battery, solid electrolyte interface, redox reaction, electrode electrolyte interface

1. Introduction

Lithium-ion batteries (LIB) have been broadly employed in portable electronic devices due to their high energy density, power density and stable performance.[1] Great focus is currently placed on applications of LIB in electric vehicles, plug-in vehicles and hybrid vehicles to fully or partially replace traditional fossil fuels and alleviate the environmental problem related to tail gas emission.[1-3] Due to its importance in modern society, the 2019 Noble Prize for Chemistry was awarded to three pioneers in LIB research. However, many open questions remain regarding chemical and electrochemical processes related to performance degradation over time. The LIB is a complex component system; multiple reactions occur during the charge and discharge processes including electrolyte and electrode degradation as well as interfacial film formation. In order to achieve better performance (i.e., higher energy and power densities, longer lifespan and stability), an in depth understanding of the working and degradation mechanisms of the LIB is imperative. Many characterization techniques have been used to study LIB electrode/electrolyte interfacial processes, such as scanning electron microscopy (SEM), transmission electron microscopy (TEM), Raman spectroscopy and electrochemical impedance spectroscopy (EIS). These techniques can provide information on morphology, chemical and structural properties as well as charge/mass transportation properties of different materials.[4-8] Scanning probe microscopy techniques, such as atomic force microscopy (AFM) and scanning tunneling microscopy (STM), can be used for imaging surfaces and characterizing surface properties of different materials.[9] However, they cannot directly monitor the electrochemical reactions occurring at the electrode/electrolyte interface during charge/discharge processes or differentiate variations in surface reactivity. SECM can overcome these typical problems as the SECM signals can be

obtained by recording the ultramicroelectrode (UME) tip current as a function of tip position over a substrate. Therefore, SECM can determine the local and real-time electrochemical activity of the reactions and provide information about topographic properties, reaction intermediates and active sites on the surface.[10-15] In 1986, Engstrom et al. employed microelectrodes to determine the electrode surface activity and detect short-lived reaction intermediates, which has been considered the first SECM-like experiment.[16, 17] The technique was further developed through the work of Bard.[18, 19] Since the first commercial SECM instrument was produced by CH Instruments in 1999, more and more researchers have conducted SECM experiments and the number of the corresponding publications increased significantly.[20] As a powerful and promising analytic tool, SECM has been widely utilized in a variety of research fields such as biology and electrochemistry.[21] As summarized in **Fig. 1**, SECM has been employed for studies of electrodes, electrolytes and solid electrolyte interfaces (SEI) in LIBs. A simple schematic illustrating the salient features of an SECM system is shown in **Fig. 2**. The system typically consists of a four-electrode electrochemical cell with an UME "tip" electrode as well as an experimental substrate electrode. The potentials and currents at the tip and substrate electrodes are controlled *vs*. the same counter and reference electrodes using a bi-potentiostat. The cell is typically filled with a desired electrolyte solution. The tip electrode can be selectively located within the cell using a three-axis translation system. A variety of techniques can be employed at the tip electrode to probe local electrochemical environments both in bulk solution as well as when placed near the active substrate/electrolyte interface.[22-25] For characterizing near surface processes, the measured signal depends on both on the electrochemical activity of the electrodes under the chosen conditions as well as the tip to substrate spacing. The use of a small tip electrode and multi-axis translation allows a degree of spatial resolution that enables imaging and identification of active or in-active

sites. In addition, the combination of small tip electrodes as well as control of tip to substrate spacing allows the examination of short-lived species that may be present near an active electrochemical interface. This combination of properties makes the SECM technique an interesting one to help gain better understanding of the interfacial electrochemistry of LIB systems.[23, 26, 27]

In this paper, we provide a brief review of SECM as an analytical tool for LIB study. The working principles of SECM are introduced, followed by the approaches and results of recent research, problems and perspectives are given finally. Through this paper, we hope to provide valuable information related to present LIB research and give a brief introduction of SECM to the people who are interested in further research in this area.
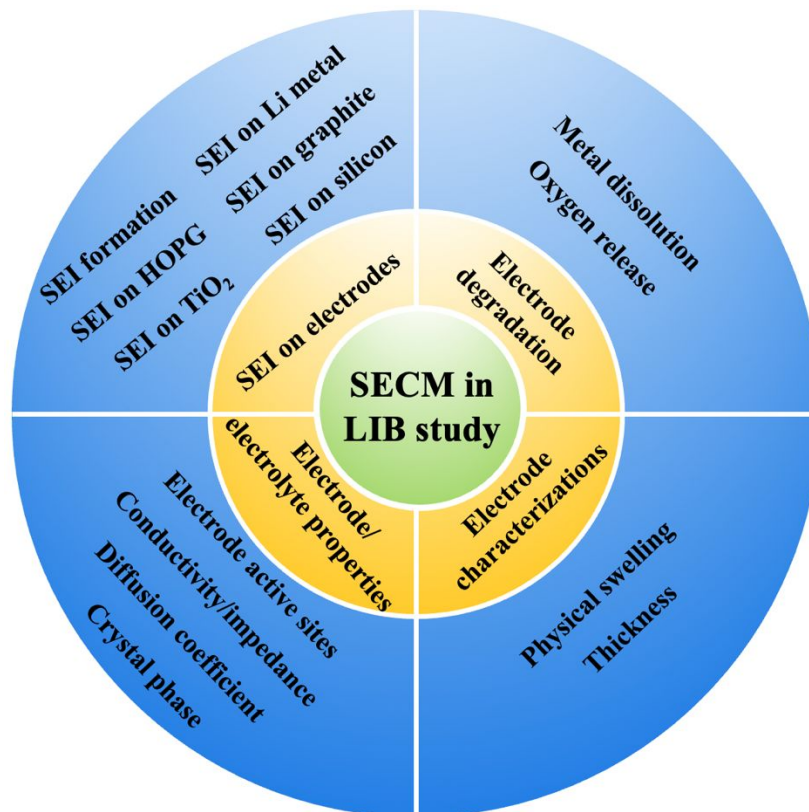

Fig. 1. SECM applications in lithium-ion batteries.

2. SECM Apparatus

Fig. 2a illustrates the setup of a basic SECM instrument (CHI920D, CH Instruments, Inc.) configured for LIB related research. The system consists of a three-electrode electrochemical cell (**Fig. 2b**). The tip and substrates act as independent working electrodes (WE) while a piece of lithium foil serves as a combined counter/quasi-reference electrode. All electrodes are immersed in electrolyte. The instrument is contained in an inert atmosphere glovebox that is filled with ultra-high purity Argon gas. The oxygen and water concentration inside are maintained at close to 0 ppm. A clear schematic of the SECM is shown in **Fig. 2c**. The position of the UME tip is controlled precisely by a combination of stepper motors for course and piezo controllers fine positioning. The tip potential and the substrate potential are controlled independently by a bi-potentiostat. The key basis of the technique is detection and characterization of electrochemical reactions (either deliberately added or natively occurring) between the tip and underlying substrate. The tip can scan across a substrate surface to differentiate active sites from inactive ones (imaging modes) or can remain at a fixed position to monitor current changes with time and potential (measurement modes). Positioning of the tip near a substrate surface can be accomplished through a variety of techniques but is commonly done by measuring how the tip current changes as it approaches the substrate while biased to drive the oxidation or reduction of a deliberately added redox mediator species under diffusion limited conditions. A convenient example of a commonly used redox mediator is Ferrocenemethanol (FcMeOH). Details of feedback mode positioning will be discussed in a later section. Data acquisition hardware is required to control the signals to the position controllers as well as collect data from the tip and substrate. The tip signal is typically generated with amperometric measurements with a detection sensitivity in the range of

picoamperes (10^{-12}A); however, the method can also be employed using potentiometric and other varied detection schemes at the tip electrode. The UME tip of SECM is commonly made of Pt, Au or C, sealed in a glass sheath ground to a fine point with the glass insulating sheath with an area approximately 10X that of active electrode area. The ratio of the area of the insulating sheath compared to the active area of the electrode is referred to as the "RG value", which plays an important part in simulation and data interpretation. The RG value can affect the SECM current response for a tip due to the blocking of mediator/reactant diffusion by the insulating shield. A tip with a smaller value of RG can allow significant diffusion around the insulator and thus will impact observed currents at the tip.[28, 29] Therefore, the RG value of the UME tip should be noted and reported in all published works. The diameter of UME tip is commonly in the range of~ micrometers but more recent work has driven this well into the nanometer range. The size of the electrode area, in part defines the resolution with which surface characterization measurements can be made, but also helps define the rate at which other electrochemical measurements can be made due to decreased capacitive background signals. This can be particularly useful when studying fast electron transfer reactions or characterizing short lived species that may evolve near a substrate surface.
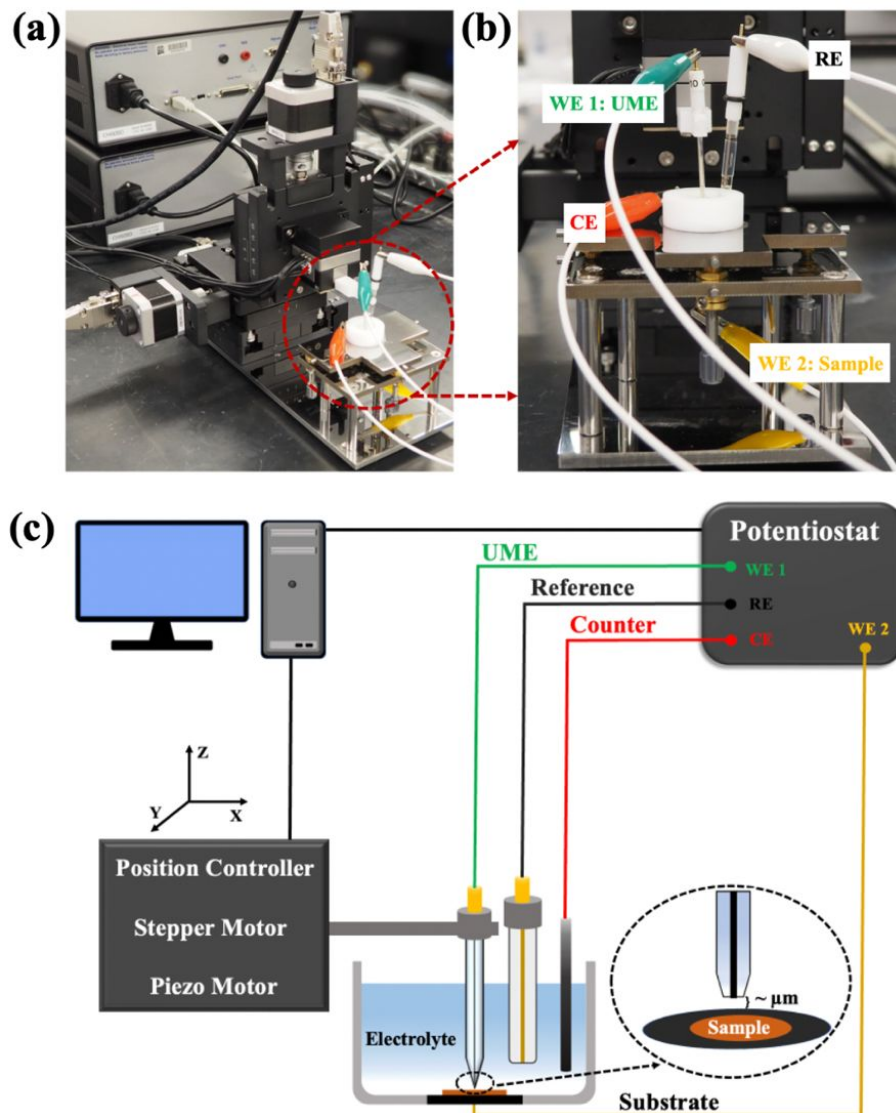
Fig. 2. (a) The setup of the SECM instrument; (b) a magnified image of the four-electrode cell; and (c) the schematic diagram of the SECM setup and electrode connections.

3. Battery Relevant SECM Modes of Use

The battery relevant operating modes of SECM can be divided into following different categories, as summarized in **Table 1** and are discussed in more detail below.

Table 1. Various working modes of SECM employed in lithium-ion battery study.

SECM modes	Redox reactions	Measurements	Applications	References
Feedback mode	$O + ne^- \rightarrow R$	Tip current	Topography and the electrochemical activity of the substrate	Ref.[30]
Tip generation/ Substrate Collection mode	$O + ne^- \rightarrow R$ (Tip) $R - ne^- \rightarrow O$	Tip and substrate currents	Reaction kinetics	Ref.[31]
Substrate generation/ Tip Collection mode	$O + ne^- \rightarrow R$ $R - ne^- \rightarrow O$ (Tip)	Tip and substrate currents	Fluxes of species generated at the substrate	Ref.[32]
Redox Competition	$O + ne^- \rightarrow R$	Tip current	Catalytic active sites of the substrate	Ref.[33]

3.1 Feedback modes

Feedback mode is the most common operating mode of SECM. These modes are based on the reactivity of a chosen redox mediator that is deliberately added to the electrolyte solution. As an example, using a generic mediator species, delineated here as "O", the tip electrode is biased to drive the diffusion limited reduction (**Eq. (1)**) where O refers to the oxidized form and R refers to reduced form of the mediator.

$$O + ne^- \rightarrow R \qquad (1)$$

With the tip electrode held in "bulk" solution, under diffusion-limited conditions, the measured steady state current at the tip designated as i_T, is defined by **Eq. (2)**:

$$i_T, = 4nFD_oC_o\alpha \qquad (2)$$

where F is the Faradic constant (96485 C mol^{-1}), D_o is the diffusion constant (cm^2 s^{-1}), C_o* is the bulk concentration of O (mol cm^{-3}) and α is the radius of the UME tip (cm in this equation). In the SECM technique, "bulk" solution is defined as at a distance greater than 10 times the radius of the tip electrode. When the tip approaches the substrate, this steady state tip current will be perturbed by the presence of the substrate. As shown in **Fig. 3a**, if the substrate is insulating or

electrochemically inactive, the measured current will decrease as compared to $i_{T,\infty}$. This is referred to as negative feedback. If the substrate is conducting or electrochemically active, R can be oxidized back to O at the substrate and allow the tip current to increase due to an increased flux of O to the tip. This is referred to as positive feedback. If this data is collected under diffusion limited electron transfer conditions the data can be fit to known working curves to estimate the tip to substrate distance.

3.2 Generation/Collection (G/C) modes

Generation/Collection modes can be divided into the Tip Generation/Substrate Collection (TG/SC) and Substrate Generation/Tip Collection (SG/TC). In a G/C mode experiment, a redox mediator is typically not included in the electrolyte solution and the technique relies on the reactivity of natively occurring redox-active species generated either at the tip or at the substrate. As an example, referring to the reaction in **Eq. (1)** $O + ne^- \rightarrow R$ and assuming O is the only reactant existing in the electrolyte, for the TG/SC mode, when a proper potential is applied to the tip, O will be reduced at the tip to generate R which will diffuse to the substrate and can be simultaneously collected to oxidize R back to O (**Fig. 3b**). Vice versa, in the SG/TC mode, R is generated from the substrate and collected by the tip (**Fig. 3c**). Using G/C method, when the tip scans across the substrate at a fixed height, it can differentiate the active sites from the inactive sites of the sample by the amplitude of measured tip current, which is useful to determine the performance of electrocatalysts.[10, 34-38] However, since the substrate has a much larger size than the tip, in SG/TC mode, the collection efficiency of the tip cannot reach 100%. Therefore, the tip is required to be close enough to the substrate to increase the efficiency (L<10). In studies from Bard's group, the substrate and the tip with the same size are applied using two Au wires with a

diameter of 12.5 μm used as the substrate and the tip.[11, 39] In this case, at close tip to substrate spacing the collection efficiency can be 100% either in TG/SC or SG/TC mode.

3.3 Redox competition mode

As shown in **Fig. 3d**, in the redox competition mode the same redox reaction happens simultaneously at the tip and the substrate. The procedure can be described briefly as follows. Apply suitable potentials to drive the relevant reaction at the tip and the substrate with the tip positioned close to the substrate ($d < α$ or $L < 1$). Allow the reaction at the tip/substrate to reach steady state. Once this is achieved, when the tip scans over the substrate, at inactive sites, the measured current will remain constant; at active sites, due to the consumption of analyte by the substrate, the measured current will be decreased. For very active sites, the reactant is depleted and the measured current drops to 0. To avoid such depletion, a pulse potential is applied to regenerate the analytes. Even though the competition mode is not utilized as much as feedback or G/C mode, it does not require minimization of the sizes of tip and substrate.[35, 40, 41] Observed contrast in this mode relies on the concentration of the analyte.
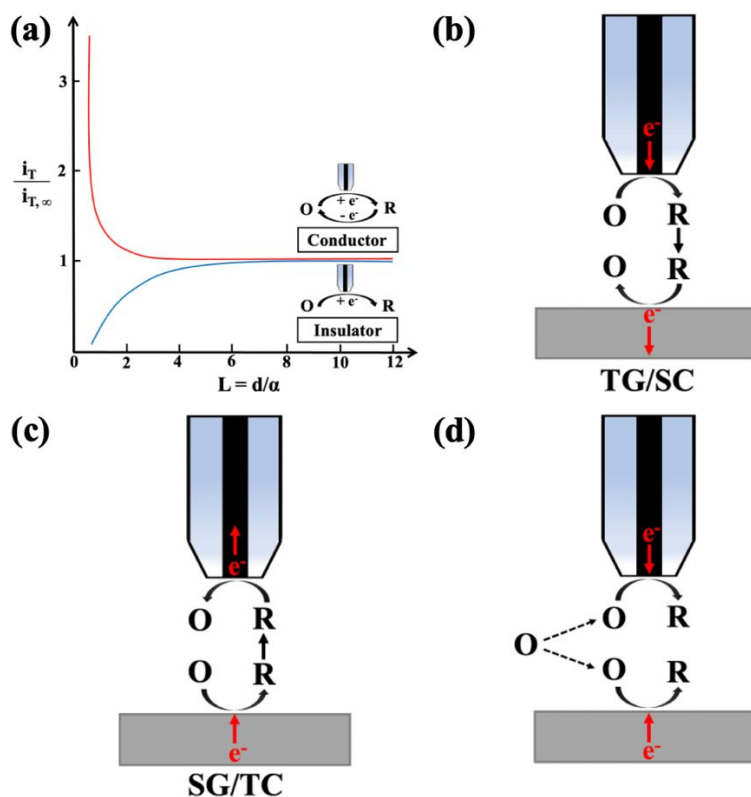
Fig. 3. SECM modes: (a) feedback mode for conductor and insulator; (b) TG/SC mode; (c) SG/TC mode and (d) redox competition mode.

4. SECM applications

4.1 Analysis of SEI in LIBs

4.1.1 SEI formation. In commercial LIBs, the negative electrode stores Li^+ at a potential close to 0 V (*vs*. Li/Li^+), the positive electrode stores Li^+ at a potential greater than 3 V (*vs*. Li/Li^+), and the electrolytes suffer from reduction at the negative electrode and oxidation at the positive electrode.[42, 43] During the first charging process, the electrolyte will go through reductive decomposition, forming a film that covers and passivates the graphite anode. This film, referred to as a "solid-electrolyte interface" (SEI) layer functions as both a Li^+ conductor and electronic insulator. A multilayer structure of the SEI has been proposed and includes a compact inner layer of inorganic salts (Li_2O, LiF and Li_2CO_3, thermodynamically stable again lithium) and porous outer layer of organic compounds stable to electrolyte (i.e. $ROCO_2Li$,).[44-47] Due to its complexity,

Peled et al have proposed a complicated mosaic model of SEI, as seen in **Fig. 4a**.[48, 49] The SEI undergoes dynamic processes with formation and dissolution happening simultaneously and significantly affects the performance of LIB, and is "the most important and the least understood in rechargeable Li batteries".[50] Detailed structure, composition, transport and kinetic properties are still unclear when different active materials are applied as electrodes. A in depth discussion of SEI formation has been given by Bard:[51] If the energy level of the electrode is higher than the LUMO (lowest unoccupied molecular orbital) of the electrolyte, electrons will be dumped into electrolyte resulting in the reduction of the electrolyte; if the HOMO (highest occupied molecular orbital) level of electrolyte is higher than Fermi level of the electrode, electrons will be transferred to the electrode and caused the oxidation of the electrolyte. The electrochemical potential difference between the negative and the positive electrodes defines the thermodynamic stability of the cell.[52] In a commercial LIB: the lithium storage potential of Li metal, graphite, Si, Sn and SiSn alloy is in the range of $0 - 1$ V (*vs.* Li/Li$^+$),[53-56] but the Fermi level is higher than the electrolyte, so using these materials as the negative electrodes leads to reduction of the electrolyte and the formation of SEI, which passivates the electrode surface and prevents the further reduction of species in the electrolyte solution.[52] A stable SEI is crucial for battery performance, and a heterogeneous SEI could induce the Li deposition nonuniformly, resulting in dendrite formation.[57-59] It has been reported that the SEI (sometimes is also called EEI; electrolyte electrode interface) could also be deposited on the positive electrode, with the same decomposition products of solvent and salt as on the negative electrode.[52, 60, 61] Oxidation of electrolyte, reactions between electrolyte and active materials, and nucleophilicity of oxygen might be involved. However, the EEIs on the positive electrode are less explored than that on the negative electrode, therefore, an operando method using SECM is critical to unveil the EEI forming mechanism at the positive electrode.

Characterization of SEI is not easy because of similar components and functional groups decomposing from the electrolyte. The sensitivity of SEI to the ambient conditions makes it difficult for most of the ex-situ characterization methods. Furthermore, the dynamic properties of the SEI require in-situ examination and SECM can be a powerful tool to study these systems.[30, 62]
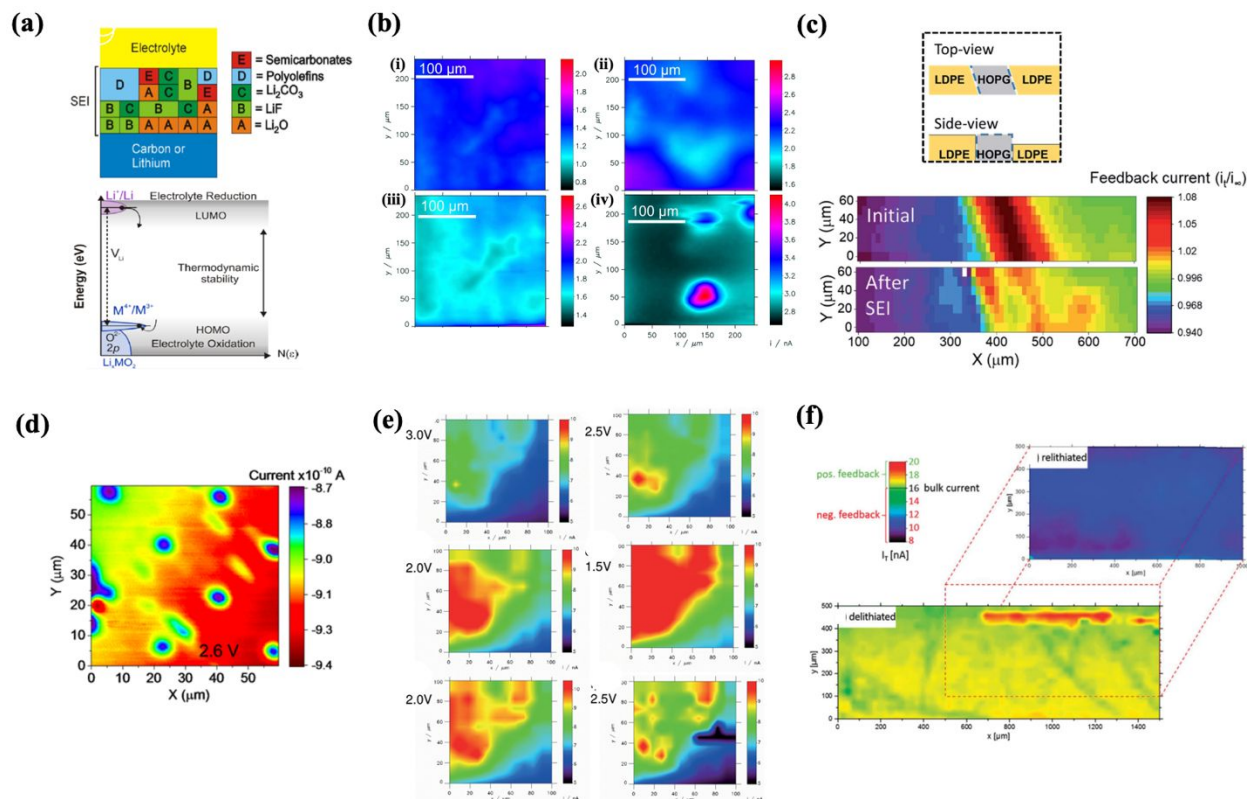
Fig. 4. (a) A mosaic model of the SEI at carbon and Lithium according to Peled (Top), [48, 49] (Reproduced from Ref. 49 with permission from John Wiley & Sons, Copyright 2016.) and electron energy levels (Bottom);[52] Reproduced from Ref. 52 with permission from American Chemical Society, Copyright 2015. (b) the SECM images showing the feedback currents before and after different charging-discharging cycles of Li metal electrode;[63] Reproduced from Ref. 63 with permission from John Wiley & Sons, Copyright 2020. (c) SECM images of current response of HOPG before and after SEI formation;[64] Reproduced from Ref. 64 with permission from the Royal Society of Chemistry, Copyright 2019. (d) the SECM image at E_{sub} 2.6 V showing good contrast between patterned holes and the multilayer graphene surface;[65] Reproduced from Ref. 65 with permission from American Chemical Society, Copyright 2016. (e) SECM feedback images of a TiO_2-based paste electrode;[66] Reproduced from Ref. 66 with permission from John Wiley & Sons, Copyright 2015. and (f) In situ SECM measurements of the Si electrode.[27] Reproduced from Ref. 27 with permission from the Royal Society of Chemistry, Copyright 2016.

4.1.2 SEI on Li metal. SECM has been extensively employed to characterize the SEI on different surfaces. Bulter et al. applied the SECM feedback mode to observe the SEI on lithium metal. 2,5-di-tert-butyl-1,4-dimethoxybenzene (DBDMB) was used as the redox mediator which was oxidized at the tip and reduced at the substrate. Unlike composites anodes in commercial LIB, for the Li anode, each Li atom on the surface possesses the same activity as others, so a homogeneous SEI layer was expected.[67] However, through SECM study, the authors proved that the inhomogeneity of SEI on Li. The results suggested that SEI formation on Li metal was a dynamic process and the release of the stress accumulated during the lithiation and delithiation impacted the formation of SEI. Similarly, Krueger et al. investigated the local protecting properties of SEI by cycling Li metal electrode in 1 M $LiClO_4$ in propylene carbonate using SECM feedback mode.[63] **Fig. 4b** showed the evolution of the SEI on Li metal by measuring the current response at different stages: (i) the Li metal before cycling; (ii) after the first charging-discharging cycle, (iii) after 6 cycles, and (iv) after 21 cycles. It was found that the SEI tends to be less protective at protruding Li deposits as a higher current was observed above the newly deposited lithium spots compared to the reference surface.[63] They also noted that the SEI passivity could change over time during the cycling due to the restructuring of surface layers. The change in SEI passivity may affect the electrode conductivity by changing its surface resistance, which may need further characterization.

4.1.3 SEI on highly oriented pyrolytic graphite (HOPG). HOPG is an interesting material for SEI study due to its strong anisotropic properties between the edge and the basal planes. Li intercalation only happens at the edge plane instead of the basal plane except for at defect sites.[68] The properties of SEI formed at the basal plane without Li^+ intercalation is very different from the one at the edge plane with Li^+ intercalation and allows separate investigation of the basal plane

and the edge plane.[69] Gossage et al. described in great detail the use of SECM feedback mode for the characterization of SEI on HOPG.[64] Linear sweep voltammetry (LSV) with a wide range of potential was used to form the SEI. The SECM images indicated the decrease in feedback current at the HOPG edge after SEI formation, suggesting that the SEI was formed at the edge site of HOPG (**Fig. 4c**). This result also revealed that HOPG edge plane is more favorable for Li^+ intercalation/de intercalation compared with its basal plane, which is attributed to the fast electron transfer kinetics and high reaction active sites.[70, 71] Another similar technique known as scanning electrochemical cell microscopy (SECCM), has been used for the characterization of SEI in LIB study.[23] SECCM coupled with a nanopipette can be used to visualize the surface reactivity of the selected areas of the electrode materials. Recently, Martín-Yerga et al. applied SECCM to study the SEI formation on HOPG of different grades with a scan rate of 1 V s^{-1}.[72] The short time measurements can reflect the formation of inorganic species in SEI at the earliest stage. The measured differences in electroactivity for different HOPG grades reveal that higher-level defects can improve the passivity and stability of SEI, leading to less electrolyte reactivity and consumption during charge and discharge processes.

4.1.4 SEI on graphite. The local electron transfer rates in the electrolyte solutions can be selectively detected by SECM.[73] Bulter et al. applied this property to characterize the local variation and temporal development of SEI properties on the graphite electrode.[74] They found that graphite composite anodes showed a local variation of electron transfer rates and temporal evolution over time, and the origin of these changes is caused by the SEI itself rather than driven by the interactions within the graphite electrode in LIBs. Furthermore, they compared the properties of SEI formed on graphite and HOPG. The results indicated that the SEI at graphite is less stable compared to HOPG, resulting from the interactions within graphite composites.[12] Hui

et al. used SECM feedback images to detect the changes on the surface conductivity of a few layers of graphene during SEI evolution (**Fig. 4d**).[65] SECM provided sufficient details of both the electronic and ionic reactivity of the graphene substrate, and illustrated the significance of the channels in enabling Li-ion intercalation, which yielded guidance for mechanistic control of ion intercalation on graphene. In addition to exploring the electrochemical properties of SEI on graphite, the evolution of SEI in long-term cycles has also been investigated by Zeng et al.[75] A nonuniform insulating SEI layer was initially formed on the electrode surface after 1 h rest time. An increase in substrate conductivity was detected after 6 h rest, probably resulting from the decomposition of SEI layers. In addition, the proportion of tip current increased with increasing rest time, indicating the expansion of SEI with time. These observations demonstrated that a long time is required for the unstable species in SEI to be converted and then stabilized on graphite surface.

4.1.5 SEI on TiO_2. Anatase TiO_2 has been widely explored as negative electrode in LIBs due to its higher theoretical Li-ion storage capacity.[76-78] The intercalation potential of Li^+ to TiO_2 is ~1.65 V (*vs*. Li/Li^+), while the deintercalation potential is 1.9 V.[79] The operation potential of TiO_2 (1.7 V) is within the stability window of carbonaceous materials, resulting in a decrease of cell energy density. This lower cell energy results in the TiO2 not being natively reactive to commonly used organic electrolytes, and it is believed that no SEI or a very thin layer of SEI forms under normal operation windows. Zampardi et al. employed a feedback mode of SECM and ferrocene as the redox mediator to explore the formation of SEI on anatase TiO_2 (**Fig. 4e**).[66] Fc^+ was produced on the tip and reduced on the TiO_2 substrate. An initial potential of 3.0 V (*vs*. Li/Li^+) was set to the substrate, then reduced by a step of 0.5 V. During Li^+ intercalation, the conductivity of TiO_2 was

increased, resulting an increase in tip current. When the potential dropped to a low level, an SEI was formed and due to its insulating property, a decrease in tip current was observed. Ventosa et al. applied SECM to determine the properties and nature of possible types of deposited solid films on anatase TiO_2 electrode surfaces.[80] Their results indicated that the SEI was detected in the potential range of 3.0 - 1.0 V (*vs*. Li/Li$^+$). Interestingly, SECM measurements demonstrated that the electrochemical reactivity of the electrode surface did not decrease, demonstrating that the solid film formed on anatase TiO_2 had conducting properties and thus the TiO_2 electrode could retain electrochemical activity. Therefore, they proposed using the term 'apparent SEI' to differentiate it from the SEI with insulating properties. Consequently, these observations demonstrated that SECM was useful for the determination of the formation potential and the electrochemical properties of solid layers on the TiO_2 electrodes.

4.1.6 SEI on Silicon. Silicon (Si) is important for Li$^+$ storage and a Si atom can store 4 Li$^+$ (Li_4Si or $Li_{15}Si_4$) in theory.[81-85] However, due to large volume change upon lithium ion intercalation (~ 400%), Si particles will crack and eventually lead to failure of the LIB. Optical microscopy can observe the cracks ex situ, but cannot determine if the cracks are formed during lithiation then become visible during delithiation, or if they are formed during delithiation. Ventosa et al. applied the SECM feedback mode using the (Fc/Fc$^+$) mediator to study the Si electrode: the potential of the tip was kept at 3.6 V (*vs*. Li/Li$^+$) and the tip was held at a constant distance (12 μm) from the substrate, as shown in **Fig. 4f**.[27] Cyclic voltammetry (CV) with the potential range from 0 to 3 V was applied to the Si substrate with a scan rate of 0.2 mV s^{-1}. In the initial cycle, during delithiation (the positive scan), a large current change was observed, showing that the as formed SEI layer (during the negative scan) apparently showed discontinuity. Upon expansion and cracking of the

Si materials, a fresh, new surface was revealed and led to the decomposition of electrolyte resulting in a change of tip current. If the SEI-free cracks were formed during the first cycle, it would be covered by newly formed SEI simultaneously, then a small or short time period current change might be observed. Their study indicated that the SEI formed on Si has insulating property and the loss in this "protecting" property of SEI is attributed to the volume expansion of Si electrode during lithiation/delithiation cycling. In contrast, Sardinha et al. explored the formation of incipient organic species in SEI on single crystalline Si without lithiation/delithiation processes.[86] By applying different potentials, it was observed that the electrode passivation reached a maximum at a potential of 1.0 V, indicating a heterogeneous growth and the nearly full coverage of SEI layers on the Si electrode. They proved that SEI could be formed on single crystalline Si electrode with high conductivity and an almost perfectly smooth surface. The examples presented above show that the initiation of SEI on Si electrode and the SEI passivity are affected by Si surface properties and the applied potentials.

4.2 Investigation of chemical species released or produced at the electrode

$LiCoO_2$ has been the major cathode material in commercial LIB since its discovery by Goodenough in 1980.[87] The theoretical capacity could reach 274 mAh g^{-1}, while the actual reversible capacity is only around 140 mAh g^{-1}.[88, 89] The possible failure mechanism are: (1) dissolution of Co from $LiCoO_2$;[90] (2) damage from strain;[91] (3) phase transition;[92] and (4) oxygen loss from $LiCoO_2$.[93] At room temperature, Snook et al. used ionic liquid 1-butyl-1-methylpyrrolidinium bis-(Trifluoromethanesulfonyl)imide (C4mpyrTFSI) as electrolyte and $LiCoO_2$ coated platinum was the cathode.[94] A SG/TC mode was applied and showed that Co^{2+} was generated from the substrate at 5.1 V (vs. Li/Li$^+$) with the tip collecting the product by CV with a

scan rate of 20 mV s^{-1} from 5.3 V to 2.6 V (*vs*. Li/Li$^+$). A complicated I – V curve was obtained

from this experiment including the process of Co dissolution and oxygen evolution. The authors

concluded that most of the dissolution of LiCoO$_2$ occurred during the deep discharge condition.

The reduction of Co^{2+} to Co$^+$ is most likely the reason for LiCoO$_2$ degradation, because Co$^+$ is

unstable in the structure and could easily move into the surrounding environment.[94] Similar metal

element dissolutions were reported in lithium manganate cathodes such as LiMn$_2$O$_4$(LMO),

Li(Ni,Mn)$_2$O$_4$ and Li(Ni,Mn,Co)O$_2$, due to the conversion of Mn^{3+} to Mn^{2+} during the

charge/discharge cycles.[95-97]
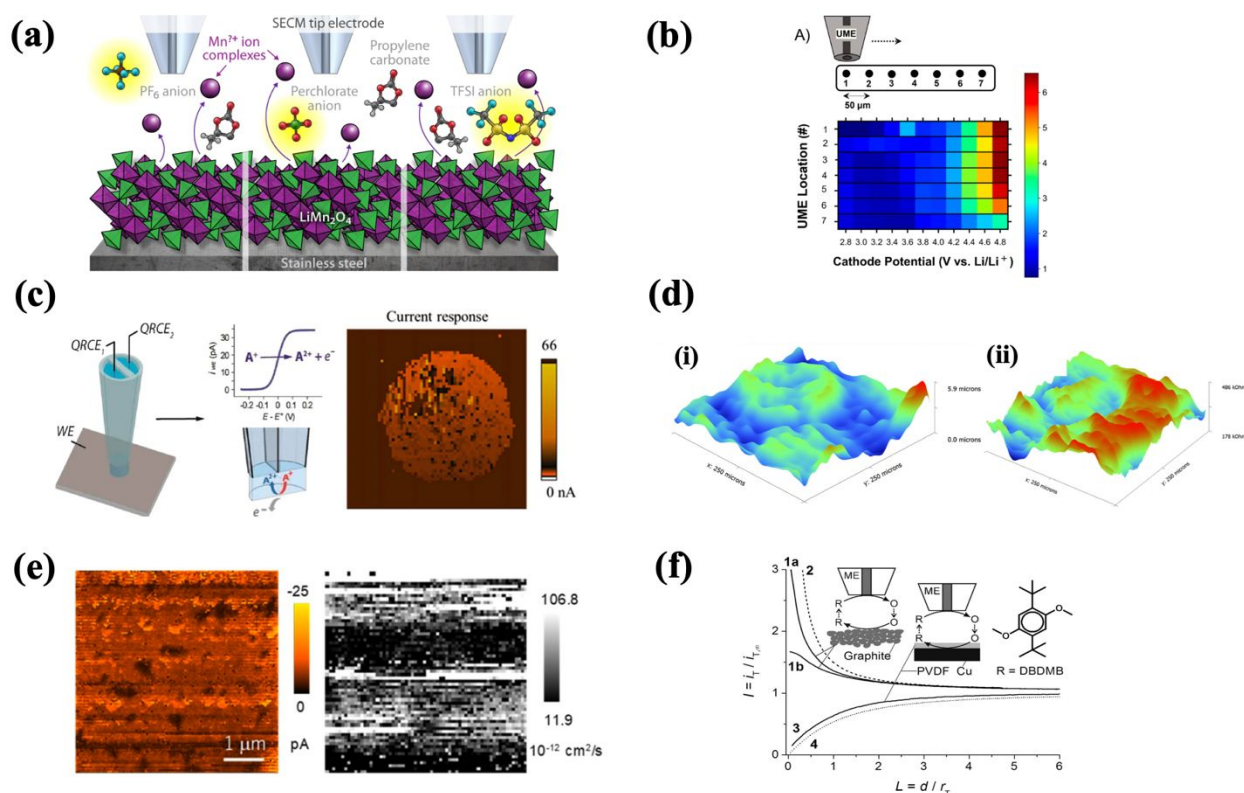
Fig. 5. (a) The monitoring of LMO degradation in varied electrolytes;[32] Reproduced from Ref. 32 with permission from American Chemical Society, Copyright 2021. (b) SECM average current plotted as a function of cathode potentials and UME position;[98] Reproduced from Ref. 98 with permission from IOP Publishing, Copyright 2022. (c) illustration of SECCM (Left)[99], Reproduced from Ref. 99 with permission from American Chemical Society, Copyright 2012; and the SECCM current image of a single LiFePO$_4$ secondary particle (Right);[100] Reproduced from Ref. 100 with permission from John Wiley & Sons, Copyright 2019. (d) topographic (i) and impedance (ii) responses of a LLZO pellet measured by ic-ac-SECM;[101] Reproduced from

Ref. 101 with permission. Copyright 2016, Frontiers. (e) SECCM current (Left) and diffusion coefficient (Right) images of the LTO electrode with a scan size of 5×5 μm²;[102] Reproduced from Ref. 102 with permission from the Royal Society of Chemistry, Copyright 2020; and (f) SECM feedback approach curves obtained from graphite electrodes at different locations using 5 mM DBDMB and 1 M LiPF6 in EC:DEC 1:1 as electrolyte solution.[103] Reproduced from Ref. 103 with permission from IOP Publishing, Copyright 2015.

Recently, we have investigated Mn dissolution from LMO by SECM combined with inductively coupled plasma (ICP) and electron paramagnetic resonance (EPR) spectroscopies. As shown in **Fig. 5a**,[32] SECM in G/C mode was performed to measure the electrochemical reactivity of LMO degradation products in different electrolytes including lithium perchlorate ($LiClO_4$), lithium hexafluorophosphate ($LiPF_6$), and lithium bis-(Trifluoromethanesulfonyl)imide (LiTFSI) in propylene carbonate (PC). The measurement results indicated that multiple active species appeared after holding the LMO substrate at 4.5 V (*vs.* Li/Li$^+$). We found that the generation of HF and HCl acids from $LiPF_6$ and $LiClO_4$ probably leads to Mn dissolution from LMO via a disproportionation reaction (**Eq. (4)**), converting Mn^{3+} to Mn^{2+} and potentially Mn^{4+}.

$$2LiMn_2O_4 + 4H^+ \Leftrightarrow 2Li^+ + Mn^{2+} + 3\lambda\text{-}MnO_2 + 2H_2O \tag{4}$$

The existence of Mn^{2+} in $LiClO_4$ and $LiPF_6$ electrolytes was confirmed via ICP and EPR by measuring the fresh electrolytes and electrolytes after the voltage hold. It is worth mentioning that the Mn dissolution was relatively slow in LiTFSI electrolyte since there was no produced acid to drive the disproportionation reaction. Our study demonstrates that SECM can be a powerful tool to characterize LMO degradation products, providing a deeper understanding of LMO degradation mechanism.

In addition to the investigation of metal dissolution from the electrode, SECM has also been used to characterize the oxygen loss behavior of transition metal oxide cathodes by Mishra et al. recently.[98] SECM measurements indicated two oxygen evolution behaviors of LCO,

$LiNi_{0.33}Mn_{0.33}Co_{0.33}O_2$ (NMC111) and $LiNi_{0.8}Mn_{0.1}Co_{0.1}O_2$ (NMC811), where a transient oxygen

loss occurred at 2.9–3.4 V (*vs.* Li/Li$^+$), while a continuous oxygen release at a more positive

potential (>3.6 V *vs.* Li/Li$^+$). They also obtained SECM mapping of average currents plotted as

a function of potential and UME tip position and observed that oxygen evolution behavior varied

in different locations (**Fig. 5b**). Consequently, the authors demonstrated that SECM was

successfully employed for the real-time detection of oxygen evolution and release from different

cathodes. This is a significant development in the characterization of the degradation behaviors of

cathode materials in LIBs, providing insights into the interfacial reactions at the electrodes during

the cycling.

4.3 Determination of electrochemical properties of electrodes/electrolytes

In addition to exploring surface reactions and interfacial properties, the electrochemical properties

of electrodes/electrolytes can provide valuable information to better understand the

electrochemical process and intrinsic performance of LIBs.[43]

4.3.1 Electrode active sites

SECCM was also developed to quantify the electrochemical behavior of active materials in an

electrochemical cell.[100] The working mechanism is similar to SECM except for adding a moveable

nanopipette (as shown in **Fig. 5c**, QRCE here refers to the quasi-reference counter electrode),

which can contact the surface of the measured sample closely.[99] The spatial resolution obtained is

two orders of magnitude better than other electrochemical imaging studies of such materials.[25, 99,

104] Kumatani et al. used SECCM to analyze the local electrochemical properties of the LiFePO$_4$

electrode and identify its active materials. The current response from Li$^+$ deintercalation process

on LiFePO$_4$ electrode is visualized in **Fig. 5c**.[100] A high current was observed over the LiFePO$_4$

particle only, indicating that LiFePO$_4$ particle provided the active sites for the reaction and

binders/additives were not active for the reaction. The SECM redox competition mode was used

by Mahankali et al to study lithium – sulfur (Li-S) batteries.[33] The experiment was performed in

Li_2S_6 solution using Pt as SECM tip and a Pt nanoparticle modified carbon electrode as substrate.

A constant potential of 2.6 V (*vs.* Li/Li^+) was applied to the tip, corresponding to the oxidation

potential of Li_2S_6. 2.5 V, 2.6 V and 2.7 V were applied to the substrate, respectively. A uniform

distribution of tip current was observed throughout the substrate with a potential of 2.5 V due to

lack of the competitive oxidation reaction on the substrate as the applied potential was not high

enough for Li_2S_6 oxidation. At 2.6 V, the tip current decreased, which was caused by the competing

oxidation of Li_2S_6 on the Pt nanoparticle modified substrate; at 2.7 V, a larger decrease in current

was observed than that of 2.6 V, due to the increased oxidation at the substrate. This result also

demonstrated that the Pt nanoparticle modified substrate was more active for Li_2S_6 oxidation than

the small Pt tip. Moreover, the non-uniform distribution of tip current indicated the co-existence

of conducting and insulating regions, corresponding the active and inactive sites on the substrate

surface.

4.3.1 Conductivity

The measurement of local impedance plays a crucial role in evaluating the electrochemical activity

of electrode materials and understanding the charge and discharge processes in LIBs. Alternating-

current SECM (ac-SECM) has been developed to measure the local conductivity and interfacial

impedance properties without use of a redox mediator.[105] By applying an oscillating potential, at

a certain frequency, local conductivity and active site concentration on the interface could be

derived.[105-107] Liu et al. employed the SECM feedback mode and ac-SECM to investigate the SEI

in aqueous LIB, unlike the SEI formed in LIB in organic electrolyte, the SEI in aqueous solution

mainly consisted of inorganic salts, which formed a discontinuous layer on the negative electrode.[108] The lithiation would increase the conductivity of TiO_2 electrode, and the positive feedback from the uncovered surface was observed, which is quite different from the SEI in organic LIBs.[108] Another creative application of the ac-SECM was demonstrated by Tallman et al. to explore the effect of metal coating on the conductivity of graphite electrode in LIBs.[109] Their results show that Ni-coated graphite has lowest impedance corresponding highest electronic conductivity, compared with untreated graphite and Cu-coated graphite. Evidently, SECM can provide information about the conductivity of the electrode before and after metal coating, making it a useful tool in the characterization of electrode materials.[109] The determination of local conductivity using SECM has extended to all-solid-state LIBs. Catarelli et al. reported that SECM can directly observe the differences in local conductivity in solid-state electrolyte, which discriminate between grain and grain boundary and obtain spatial information simultaneously.[101] Intermittent contact alternating current SECM (ic-ac-SECM) was applied to characterize Al-substituted $Li_7La_3Zr_2O_{12}$ (Al-LLZO), which is an electrolyte in solid state LIB. Impedance mapping implied that significant variation in resistance was observed between the grain and grain boundaries (**Fig. 5d**), as well as in grain boundaries themself, resulting from the difference of the grain boundary structure and chemistry.[101]

4.3.2 Diffusion coefficient and crystal phase

The determination of kinetic parameters of the LIBs is significantly important to understand its working mechanism and electrochemical behavior of the electrode materials. This is not easy to achieve for most commonly used characterization techniques. Takahashi et al. attempted to visualize the electrochemical reactivity and the diffusion behavior of LIB electrodes using SECCM.[102] The differences in CV response at $Li_4Ti_5O_{12}$ (LTO) and $LiCoO_2$ (LCO) electrodes

were attributed to diffusion coefficients. The Li^+ diffusion coefficient (D, cm^2s^{-1}) can be estimated by the Randles−Sevcik equation (**Eq. (5)**). The peak current i_p (A) is dependent on the concentration C ($mol\ cm^{-3}$), diffusional properties of electrolyte as well as the scan rate v ($V\ s^{-1}$) where n refers to the electron transfer number, F is the Faraday constant ($C\ mol^{-1}$), and A is the electrode area (cm^2).

$$i_p = 0.4463\ nFAC\left(\frac{nFvD}{RT}\right)^{1/2} \tag{5}$$

Fig. 5e presents the different responses in current and diffusion coefficient for LTO electrode, which is attributed to different crystal facets.[102] Moreover, Takahashi characterized the metastable state of $LiFePO_4$ (LFP) and found that the oxidation and reduction current double peaks were observed with a slow CV scan rate. The current response at around 3.4 V (*vs*. Li/Li^+) was identified as the metastable state of Li_xFePO_4. This work showed that SECCM measurements can visualize diffusion coefficients and detect the crystal phase of electrodes in LIBs.

An example of the strengths of SECM to determine the kinetic parameters of LIBs was demonstrated by Hossain et al., who applied SECM to measure the effective diffusivity of lithium using LFP as electrode.[110] They investigated the correlation between lithium diffusivity and the electrode porosity by determining the ratio of the diffusion coefficient between bulk solution and a porous electrode material. The diffusivity measurements indicated that the significant deviation was observed for the electrode with a porosity below 60%. Evidently, SECM can work as a reliable analytical tool for characterizing the reaction kinetics for LIBs. The lithium transport through the electrolyte/porous electrodes is a significant factor to achieve its high performance. Therefore, the ability of SECM to quantify lithium's diffusion characteristics can help to provide a more quantitative understanding of electrochemical behaviors of LIBs.

## 4.4 Characterization of physical swelling and thickness

The physical swelling of the graphite composite electrode in LIB was determined in situ and locally by SECM, through the approach curves of the feedback mode.[103] In **Fig. 5f**, 2,5-di-*tert*-butyl-1,4-dimethoxybenzene (DBDMB) was used as a redox mediator and was oxidized to DBDMB$^+$ at the tip and reduced back at the graphite composite electrode (81wt. % graphite, 6 wt.% carbon black, and 13 wt.% PVDF).[103] Tip approach curves were collected over the graphite composite at different locations. In the composite material, Polyvinylidene fluoride (PVDF) as the binder presents electrically insulating properties leading to negative feedback while graphite and carbon black show conducting properties leading to positive feedback. The authors mentioned that the PVDF swelling is the main cause for the physical swelling of graphite electrodes. Appropriate feedback approach curve techniques can be used to measure the difference between physical swelling and electrochemical swelling (lithiation) of the composite anode. Changes in apparent tip to substrate spacing indicated by changes in either positive or negative feedback can be observed with or without applying a potential to the composite. It is important to note that swelling already started when electrolyte was added to the system, but still while the alignment and approach of the tip to the substrate was on going were not able be measured. In addition, swelling occurs in three dimensions, however, this technique only observed the change along the z direction (thickness).

Recently, Menzel et al. reported the volume change of activated carbon electrodes in aqueous electrolytes can be characterized by SECM.[111] The SECM measurements were performed by scanning a certain part of the electrode in Li_2SO_4 solution with $K_3Fe(CN)_6$ mediator. They explained that the change in tip currents before and after electrode polarization can reflect the difference in electrode thickness. Their study confirmed the volumetric expansion of the carbon electrode after deep polarization, as a result of electrolyte adsorption and electrochemical reactions

on electrode surface. In LIBs, the mechanical stability of the electrode during cycling is of great concern and the real-time measurement of electrode swelling is still challenging. This approach would have the potential to study the expansion of different electrode materials in LIBs.

5. Other developed SECM-based techniques

The rapid development of SECM is incredibly helpful in LIB research. However, in a traditional SECM, the measured current is affected not only by the material activity. Other factors such as the structural changes during reactions (e.g., dissolution or deposition) may modify the distance of the tip to the substrate, resulting in incorrect interpretation. Integration of the SECM with other techniques that allow independent determination of substrate morphology changes may achieve interesting results, for instance, the combination of AFM and SECM can directly correlate the surface activity with the surface morphology in a single experiment. The changes of electrochemical properties and topology are related and deconvoluted separately, which is difficult to be achieved using more established SECM techniques.[74, 80, 112, 113] Zampardi et al. applied AFM-SECM to characterize the SEI layers in LIBs.[114] The SEI thickness on glassy carbon measured by AFM was ~ 30 nm. AFM tip was also operated to scratch the formed SEI layer, and the activities of SEI and non-SEI surface areas were compared. AFM − SECM has also been applied to study Li − S batteries. In one example, Li_2S and Li_2S_2 were first deposited on a carbon surface at 1.9 V forming a conducting region (Li_2S_2) and an insulating region (Li_2S). The conducting region dissolved at a high potential, while the insulating region reacted with the intermediate lithium polysulfides (LiPS), forming inactive products, and accumulating on the surface, resulting in topology change and capacity fading. A schematic drawing and simultaneous measurements of topography, current and phase are displayed in **Fig. 6a**.[33] The combination of Raman and SECM provides a direct technique to examine electrochemical properties together with spectrochemical

analysis.[115-117] Schorr et al. applied Raman-SECM using ferricyanide as mediator to study the graphene interfacial reactions and determined the real-time correlation between structural changes and measured current response (**Fig. 6b**).[118] This technique has also been employed to investigate the oxygen evolution activity of Ni/Fe electrodes.[119] The ability of Raman-SECM to provide both spectroscopic and electrochemical information gives it great potential for material characterization in LIBs. SECM coupled with Fourier-transformed infrared spectroscopy (FTIR-ATR) has been used for in situ used for studying the electrochemically induced processes in the aqueous environment, which can simultaneously obtain the SECM feedback current and IR absorption spectra. A schematic of the FT-IR-ATR setup is shown in **Fig. 6c**.[120] Interestingly, Dorfi et al. invented a continuous line probe (CLP) for SECM, consisting of one electroactive layer sandwiched by the thin insulator and a thick substrate, as exhibited in **Fig. 6d**.[121] The imaging resolution was determined by the thickness of the electroactive layer and the imaging rates were affected by its width. A high imaging rate can be achieved by such a design and the scan angle can be rotated from 0 to 360°, which is not affected by convection limitations. These hybrid techniques would enable kinetic studies on electrochemical and interfacial reactions at various surfaces, providing other chemical specificity in addition to electrochemical activity via SECM. With the further development of advanced probe technologies, multiple combinations of SECM with other advanced equipment will certainly show up. New testing methods and working mechanisms are of great interests to electrochemists. We will continue watching new developments which will provide useful information for the broader electrochemical community.
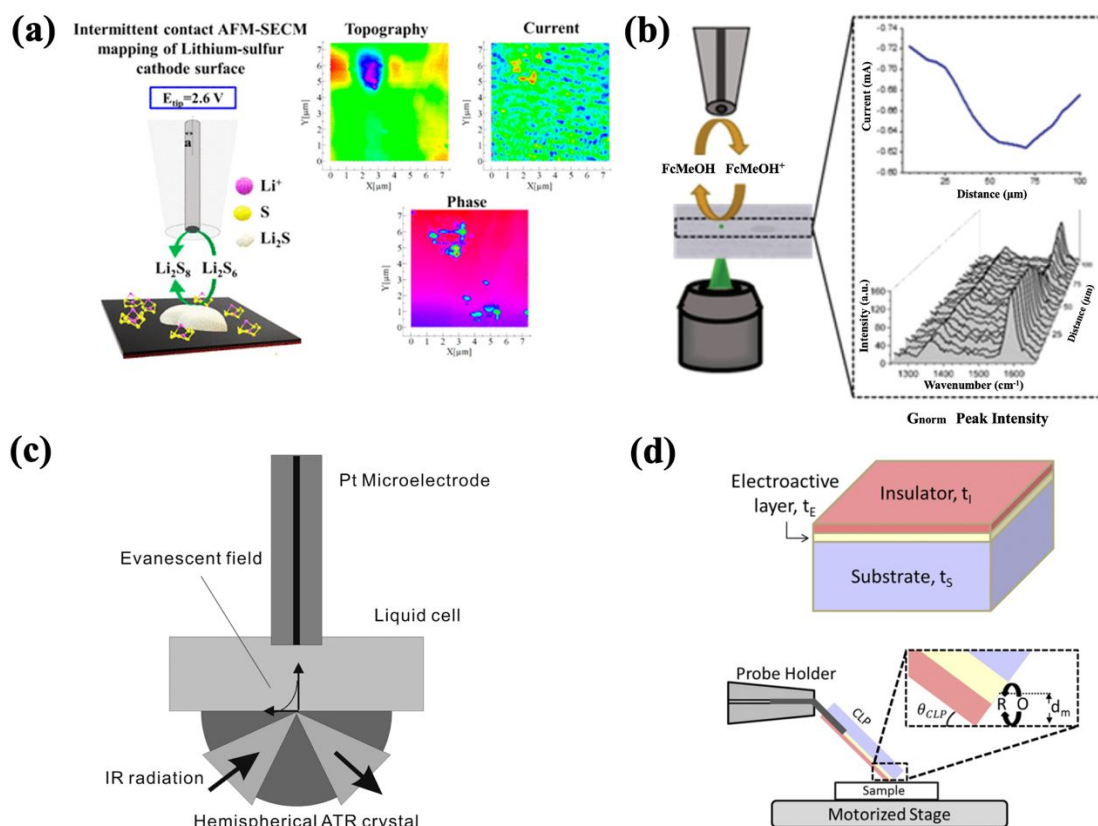
Fig. 6. (a) Schematic drawing of AFM-SECM and its combined measurements of topography, current and phase;[33] Reproduced from Ref. 33 with permission from American Chemical Society, Copyright 2019. (b) illustration of the alignment between the laser line and SECM probe. The feedback current and spectra of a single scan were obtained by scanning the x-direction and collecting the data in 100 s;[118] Reproduced from Ref. 118 with permission from American Chemical Society, Copyright 2018. (c) The scheme of the SECM- FTIR -ATR setup;[120] Reproduced from Ref. 120 with permission from American Chemical Society, Copyright 2010. (d) Schematic representations of CLP-SECM.[121] Reproduced from Ref. 121 with permission from American Chemical Society, Copyright 2019.

6. Redox mediators

SECM can provide information on both the chemical and electrochemical reactivity of electrode/electrolyte interfacial regions as well as characterize near surface transient reaction species. Several studies discussed here have used feedback mode techniques which rely on the use of a redox mediator system to both probe the surface as well as determine tip to substrate spacing in ideal circumstances.[64, 122] A suitable redox mediator usually presents the advantages of (1) the ability to react with the sample of interest (oxidation/reduction); (2) the good stability of both the

oxidized/reduced species; (3) high compatibility with the environment; and (4) high diffusivity. Several molecules/atoms have been utilized or developed as redox mediators in SECM measurements. Polcari et al. reported a comprehensive summary of redox mediators used in SECM from 1989 to 2015,[21] where details of redox reactions, solvents, the standard redox potentials, and SECM applications were given. **Table 2** provides information about mediators that have been used in SECM measurements for LIB studies. It is important to note that the properties of the studied electrodes and the mode of SECM used influence the selection of mediators. Therefore, detailed characterization of how those species interact with various LIB components is required before meaningful data and high-quality SECM images can be obtained. There likely remains a substantial need for further research toward the development of appropriate mediators in this area of research.

Table 2. Redox Mediators used in lithium-ion battery study.

Electrodes	Mediators	SECM modes	Applications	References
Li metal	2,5-di-tert-butyl-1,4, dimethoxybenzene (DBDMB)	Feedback mode	SEI	Ref. [63, 67]
HOPG	2,5-di-tert-butyl-1,4, dimethoxybenzene (DBDMB)	Feedback mode	SEI	Ref. [12]
HOPG	Ferrocene (Fc)	Feedback mode	SEI	Ref. [64]
Graphite	N,N,N',N'-tetramethyl p-phenylenediamine (TMPD)	Feedback mode	SEI	Ref. [65]
Graphite	Ferrocene (Fc)	Feedback mode	SEI	Ref. [75]
Graphite	Methyl phthalimide (PHT)	Feedback mode	SEI	Ref. [123]
Graphite	2,5-di-tert-butyl-1,4, dimethoxybenzene (DBDMB)	Feedback mode	Electrode swelling	Ref. [103]
TiO_2	Ferrocene (Fc)	Feedback mode	SEI	Ref. [66, 80]
Si	Ferrocene (Fc)	Feedback mode	SEI	Ref. [27]
Si	2,5-di-tert-butyl-1,4-dimethoxybenzene (DBDMB)	Feedback mode	SEI	Ref. [86]
Li-S	Cobaltocene	Competition mode	Electrode property	Ref. [33]
LCO	Ferrocene (Fc)	SG/TC mode	Electrode degradation	Ref. [94]
LMO	Ferrocene (Fc)	SG/TC mode	Electrode degradation	Ref. [32]
LMO	Potassium ferricyanide ($K_3Fe(CN)_6$)	Feedback mode	Cathode electrolyte interface (CEI)	Ref. [124]

7. Conclusions and perspectives

The interest in exploring how to enhance electrochemical performance of LIBs has attracted more and more attention due to the urgent demands for renewable power sources and great market potential. SECM as a powerful characterization technique can probe a variety of electrochemical processes occurring at LIB electrode/electrolyte interfaces and provide us a deeper fundamental understanding of LIBs degradation mechanisms. SECM has the advantages of (1) direct quantification and time-resolved detection of active sites and intermediates; (2) the ability to characterize the SEI properties at the LIB electrodes, which relates to surface processes, and

provide information on spatially resolved visualization of the performance of the LIB electrodes, which relates to bulk processes; and (3) the ability to detect minute changes in electrochemical reactivity near the substrate surface due to low detection current limits. In this review, we summarized that SECM can be utilized to investigate the chemical species released or produced at LIB electrode/electrolyte interfaces, to determine electrochemical/physical properties, and to explore the chemical properties of the SEI formed on the surface of different electrodes including Li metal, HOPG, graphite, TiO_2 and Si. We also gave examples to show that the local conductivity, diffusion coefficient and the binder physical swelling could be observed and determined by SECM. These studies prove that SECM is a powerful technique that can provide valuable and unique information about interfacial reactions between electrode and electrolyte and SEI in LIBs.

LIBs are complex systems with various processes that occur simultaneously. Despite great efforts, for the opportunities that SECM can offer to be fully realized the following problems still remain. Since the tip-to-substrate distance control is critical important, further methods to decouple distance measurements from electrochemical signals should be investigated. Furthermore, more effort should be devoted to increase the resolution of SECM mappings in some of the operating modes of SECM, such as feedback mode. In addition, there is a critical need to get reliable kinetic data which can help to understand the mechanism of complex reaction processes. EEI could also be formed at the cathode; it might have the same formation mechanism and composition as SEI on the anode, playing a critical role in LIB performance. However, the research of EEI on the cathode is rarely reported, especially the results based on SECM measurements. SECM has great potential to confirm the EEI formation and study its composition, properties and stability. Further studies of SECM are underway to develop the potential of SECM to contribute to LIB fields.

Acknowledgements

Competing interests

The authors declare that there are no competing interests regarding the publication of this article.

References

1   M. Li, J. Lu, Z. Chen and K. Amine. 30 Years of Lithium-Ion Batteries. *Adv. Mater.*, 2018, e1800561.

2   G. Chen, L. Yan, H. Luo and S. Guo. Nanoscale Engineering of Heterostructured Anode Materials for Boosting Lithium-Ion Storage. *Adv. Mater.*, 2016, **28**, 7580-7602.

3   J. B. Goodenough and K. S. Park. The Li-ion rechargeable battery: a perspective. *J. Am. Chem. Soc.*, 2013, **135**, 1167-1176.

4   R. Xu, J. Yue, S. Liu, J. Tu, F. Han, P. Liu and C. Wang. Cathode-Supported All-Solid-State Lithium− Sulfur Batteries with High Cell-Level Energy Density.pdf. *ACS Energy Lett.*, 2019, **4**, 1073-1079.

5   Y. Xu, K. Wood, J. Coyle, C. Engtrakul, G. Teeter, C. Stoldt, A. Burrell and A. Zakutayev. Chemistry of Electrolyte Reduction on Lithium Silicide. *J. Phys. Chem. C.*, 2019, **123**, 13219-13224.

6   M. Yoshio, H. Wang, K. Fukuda, Y. Hara and Y. Adachi. Effect of Carbon Coating on Electrochemical Performance of Treated natural graphite as lithium-ion battery anode material. *J. Electrochem. Soc.*, 2000, **147**, 1245-1250.

7   D. Xie, J. Zhang, G. Pan, H. Li, S. Xie, S. Wang, H. Fan, F. Cheng and X. Xia. Functionalized N-Doped Carbon Nanotube Arrays: Novel Binder-Free Anodes for Sodium-Ion Batteries. *ACS Appl. Mater. Interf.*, 2019, **11**, 18662-18670.

8   S. Hy, Felix, Y.-H. Chen, J.-Y. Liu, J. Rick and B.-J. Hwang. In situ surface enhanced Raman spectroscopic studies of solid electrolyte interphase formation in lithium ion battery electrodes. *J. Power Sources*, 2014, **256**, 324-328.

9   B. Voigtländer. Scanning probe microscopy- Atomic force microscopy and scanning tunneling microscopy. *Berlin: Springer*, 2015.

10   J. H. Bae, Y. Yu and M. V. Mirkin. Scanning Electrochemical Microscopy Study of Electron-Transfer Kinetics and Catalysis at Nanoporous Electrodes. *J. Phys. Chem. C.*, 2016, **120**, 20651-20658.

11   H. S. Ahn and A. J. Bard. Surface interrogation of CoP(i) water oxidation catalyst by scanning electrochemical microscopy. *J. Am. Chem. Soc.*, 2015, **137**, 612-615.

12   H. Bülter, F. Peters and G. Wittstock. Scanning Electrochemical Microscopy for the In Situ Characterization of Solid-Electrolyte Interphases: Highly Oriented Pyrolytic Graphite versus Graphite Composite. *Energy Technol.*, 2016, **4**, 1486-1494.

13   H. S. Ahn and A. J. Bard. Surface Interrogation Scanning Electrochemical Microscopy of Ni(1-x)Fe(x)OOH (0 < x < 0.27) Oxygen Evolving Catalyst: Kinetics of the "fast" Iron Sites. *J. Am. Chem. Soc.*, 2016, **138**, 313-318.

14   Y. Wu and N. Liu. Visualizing Battery Reactions and Processes by Using In Situ and In Operando Microscopies. *Chem*, 2018, **4**, 438-465.

15   P. Bertoncello. Advances on scanning electrochemical microscopy (SECM) for energy. *Energy Environ. Sci.*, 2010, **3**.

16   R. C. Engstrom, M. Weber, D. J. Wunder, R. Burgess and S. Winquist. Measurements within the Diffusion Layer Using a Microelectrode Probe. *Anal. Chem.*, 1986, **58**, 844-848.

17   R. C. Engstrom, T. Meaney, R. Tople and R. M. Wightman. Spatiotemporal description of the diffusion layer with a microelectrode probe. *Anal. Chem.* , 1987, **59**, 2005-2010.

18   D. Mandler and A. J. Bard. Scanning Electrochemical Microscopy: The Application of the Feedback Mode for High Resolution Copper Etching. *J. Electrochem. Soc.*, 1989, **136**, 3143.

19   A. J. Bard, F. Ren, F. Fan, J. Kwak and O. Lev. Scanning Electrochemical Microscopy. Introduction and principles. *Anal. Chem.*, 1989, **61**, 132-138.

20   P. Sun, F. O. Laforge and M. V. Mirkin. Scanning electrochemical microscopy in the 21st century. *Phys. Chem. Chem. Phys.*, 2007, **9**, 802-823.

21   D. Polcari, P. Dauphin-Ducharme and J. Mauzeroll. Scanning Electrochemical Microscopy: A Comprehensive Review of Experimental Parameters from 1989 to 2015. *Chem. Rev.*, 2016, **116**, 13234-13278.

22   H. Bülter, P. Schwager, D. Fenske and G. Wittstock. Observation of Dynamic Interfacial Layers in Li-Ion and Li-O2 Batteries by Scanning Electrochemical Microscopy. *Electrochim. Acta*, 2016, **199**, 366-379.

23   E. Ventosa and W. Schuhmann. Scanning electrochemical microscopy of Li-ion batteries. *Phys Chem Chem Phys*, 2015, **17**, 28441-28450.

24   C. G. Zoski. Review—Advances in Scanning Electrochemical Microscopy (SECM). *J. Electrochem. Soc.*, 2015, **163**, H3088-H3100.

25   C. L. Bentley, M. Kang and P. R. Unwin. Scanning Electrochemical Cell Microscopy: New Perspectives on Electrode Processes in Action. *Curr. Opin. Electrochem.*, 2017, **6**, 23-30.

26   D. Xia, R. Zhu, Y. Behnamian, J. Luo, C. Lin and S. Klimas. Understanding the interaction of thiosulfate with Alloy 800 in aqueous chloride solutions using SECM. *J. Electroanal. Chem.*, 2015, **744**, 77-84.

27   E. Ventosa, P. Wilde, A. H. Zinn, M. Trautmann, A. Ludwig and W. Schuhmann. Understanding surface reactivity of Si electrodes in Li-ion batteries by in operando scanning electrochemical microscopy. *Chem. Commun.*, 2016, **52**, 6825-6828.

28   K. Leonhardt, A. Avdic, A. Lugstein, I. Pobelov, T. Wandlowski, M. Wu, B. Gollas and G. Denuault. Atomic force microscopy-scanning electrochemical microscopy: influence of tip geometry and insulation defects on diffusion controlled currents at conical electrodes. *Anal. Chem.*, 2011, **83**, 2971-2977.

29   Y. Lee, S. Amemiya and A. J. Bard. Scanning Electrochemical Microscopy. 41. Theory and Characterization of Ring Electrodes. *Anal. Chem.*, 2001, **73**, 2261-2267.

30   H. Bulter, F. Peters, J. Schwenzel and G. Wittstock. Spatiotemporal changes of the solid electrolyte interphase in lithium-ion batteries detected by scanning electrochemical microscopy. *Angew Chem Int Ed Engl*, 2014, **53**, 10531-10535.

31   F. Zhou, P. R. Unwin and A. J. Bard. Scanning electrochemical microscopy. 16. Study of second-order homogeneous chemical reactions via the feedback and generation:collection modes. *J. Phys. Chem.*, 1992, **96**, 4917-4924.

32   D. Huang, C. Engtrakul, S. Nanayakkara, D. W. Mulder, S.-D. Han, M. Zhou, H. Luo and R. C. Tenent. Understanding Degradation at the Lithium-Ion Battery Cathode/Electrolyte Interface: Connecting Transition-Metal Dissolution Mechanisms to Electrolyte Composition. *ACS Appl. Mater. Interfaces*, 2021, **13**, 11930-11939.

33   K. Mahankali, N. K. Thangavel and L. M. Reddy Arava. In Situ Electrochemical Mapping of Lithium-Sulfur Battery Interfaces Using AFM-SECM. *Nano Lett.*, 2019, **19**, 5229-5236.

34   S. Kuss, D. Trinh, L. Danis and J. Mauzeroll. High-speed scanning electrochemical microscopy method for substrate kinetic determination: method and theory. *Anal. Chem.*, 2015, **87**, 8096-8101.

35   K. Eckhard, X. Chen, F. Turcu and W. Schuhmann. Redox competition mode of scanning electrochemical microscopy (RC-SECM) for visualisation of local catalytic activity. *Phys. Chem. Chem. Phys.*, 2006, **8**, 5359-5365.

36   K. Karnicka, K. Eckhard, D. A. Guschin, L. Stoica, P. J. Kulesza and W. Schuhmann. Visualisation of the local bio-electrocatalytic activity in biofuel cell cathodes by means of redox competition scanning electrochemical microscopy (RC-SECM). *Electrochem. Commun.*, 2007, **9**, 1998-2002.

37   J. L. Fernández and A. J. Bard. Scanning Electrochemical Microscopy. 47. Imaging Electrocatalytic Activity for Oxygen Reduction in an Acidic Medium by the Tip Generation−Substrate Collection Mode. *Anal. Chem.*, 2003, **75**, 2967-2974.

38   W. Schulte, S. Liu, I. Plettenberg, S. Kuhri, W. Lüke, W. Lehnert and G. Wittstock. Local Evaluation of Processed Membrane Electrode Assemblies by Scanning Electrochemical Microscopy. *J. Electrochem. Soc.*, 2017, **164**, F873-F878.

39   C. M. Sa´nchez-Sa´nchez, J. Rodrı´guez-Lo´pez and A. J. Bard. Scanning Electrochemical Microscopy. 60. Quantitative Calibration of the SECM Substrate Generation/Tip Collection Mode and Its Use for the Study of the Oxygen Reduction Mechanism. *Anal. Chem.*, 2008, **80**, 3254-3260.

40   L. Guadagnini, A. Maljusch, X. Chen, S. Neugebauer, D. Tonelli and W. Schuhmann. Visualization of electrocatalytic activity of microstructured metal hexacyanoferrates by means of redox competition mode of scanning electrochemical microscopy (RC-SECM). *Electrochim. Acta*, 2009, **54**, 3753-3758.

41   I. Morkvenaite-Vilkonciene, A. Ramanaviciene, P. Genys and A. Ramanavicius. Evaluation of Enzymatic Kinetics of GOx-based Electrodes by Scanning Electrochemical Microscopy at Redox Competition Mode. *Electroanalysis*, 2017, **29**, 1532-1542.

42   G. Crabtree, E. Kócs and L. Trahey. The energy-storage frontier: Lithium-ion batteries and beyond. *MRS Bull.*, 2015, **40**, 1067-1078.

43   R. Kempaiah, G. Vasudevamurthy and A. Subramanian. Scanning probe microscopy based characterization of battery materials, interfaces, and processes. *Nano Energy*, 2019, **65**, 103925.

44   A. Wang, S. Kadam, H. Li, S. Shi and Y. Qi. Review on modeling of the anode solid electrolyte interphase (SEI) for lithium-ion batteries. *NPJ Comput. Mater.*, 2018, **4**, 1-26.

45   S. J. An, J. Li, C. Daniel, D. Mohanty, S. Nagpure and D. L. Wood. The state of understanding of the lithium-ion-battery graphite solid electrolyte interphase (SEI) and its relationship to formation cycling. *Carbon*, 2016, **105**, 52-76.

46   Y. Geronov, F. Schwager and R. H. Muller. Electrochemical Studies of the Film Formation on Lithium in Propylene Carbonate Solutions under Open-Circuit Conditions. *J. Electrochem. Soc.*, 1982, **129**, 1422-1429.

47   K. Kanamura, H. Tamura, S. Shiraishi and Z. i. Takehara. XPS Analysis of Lithium Surfaces Following Immersion in Various Solvents Containing LiBF4. *J. Electrochem. Soc.*, 1995, **142**, 340-347.

48   E. Peled, D. Golodnitsky and G. Ardel. Advanced Model for Solid Electrolyte Interphase Electrodes in Liquid and Polymer Electrolytes. *J. Electrochem. Soc.*, 1997, **144**, L208-L210.

49   P. Schwager, H. Bülter, I. Plettenberg and G. Wittstock. Review of Local In Situ Probing Techniques for the Interfaces of Lithium-Ion and Lithium-Oxygen Batteries. *Energy Technol.*, 2016, **4**, 1472-1485.

50   M. Winter. The Solid Electrolyte Interphase – The Most Important and the Least Understood Solid Electrolyte in Rechargeable Li Batteries. *Z. Phys. Chem.*, 2009, **223**, 1395-1406.

51   A. J. Bard and M. V. Mirkin, *Scanning electrochemical microscopy*, CRC Press, 2012.

52   M. Gauthier, T. J. Carney, A. Grimaud, L. Giordano, N. Pour, H. H. Chang, D. P. Fenning, S. F. Lux, O. Paschos, C. Bauer, F. Maglia, S. Lupart, P. Lamp and Y. Shao-Horn. Electrode-electrolyte interface in Li-ion batteries: current understanding and new insights. *J. Phys. Chem. Lett.*, 2015, **6**, 4653-4672.

53   R. Yazami and P. Touzain. A reversible graphite-lithium negative electrode for electrochemical generators. *J. Power Sources*, 1983, **9**, 365-371.

54   K. Ji, J. Han, A. Hirata, T. Fujita, Y. Shen, S. Ning, P. Liu, H. Kashani, Y. Tian, Y. Ito, J. I. Fujita and Y. Oyama. Lithium intercalation into bilayer graphene. *Nat. Commun.*, 2019, **10**, 1-10.

55   J. Wang, I. D. Raistrick and R. A. Huggins. Behavior of Some Binary Lithium Alloys as Negative Electrodes in Organic Solvent-Based Electrolytes. *J. Electrochem. Soc.*, 1986, **133**, 457-460.

56   J. Graetz, C. C. Ahn, R. Yazami and B. Fultz. Highly Reversible Lithium Storage in Nanostructured Silicon. *Electrochem. Solid-State Lett.*, 2003, **6**, A194-A197.

57   G. Yang, Y. Li, Y. Tong, J. Qiu, S. Liu, S. Zhang, Z. Guan, B. Xu, Z. Wang and L. Chen. Lithium Plating and Stripping on Carbon Nanotube Sponge. *Nano. Lett.*, 2019, **19**, 494-499.

58   F. Nobili, M. Mancini, S. Dsoke, R. Tossici and R. Marassi. Low-temperature behavior of graphite–tin composite anodes for Li-ion batteries. *J. Power Sources*, 2010, **195**, 7090-7097.

59   T. Liu, J. Hu, C. Li and Y. Wang. Unusual Conformal Li Plating on Alloyable Nanofiber Frameworks to Enable Dendrite Suppression of Li Metal Anode. *ACS Appl. Energy Mater.*, 2019, **2**, 4379-4388.

60   Y. Lu, H. A. Gasteiger, M.C. Parent, V. Chiloyan and Y. Shao-Horn. The Influence of Catalysts on Discharge and Charge Voltages of Rechargeable Li–Oxygen Batteries. *Electrochem. Solid-State Lett.*, 2010, **13**.

61   R. V. Chebiam, A. M. Kannan, F. Prado and A. Manthiram. Comparison of the chemical stability of the high energy density cathodes of lithium-ion batteries. *Electrochem. Commun.*, 2001, **3**, 624-627.

62   G. Wittstock, M. Burchardt, S. E. Pust, Y. Shen and C. Zhao. Scanning electrochemical microscopy for direct imaging of reaction rates. *Angew. Chem. Int. Ed.*, 2007, **46**, 1584-1617.

63   B. Krueger, L. Balboa, J. F. Dohmann, M. Winter, P. Bieker and G. Wittstock. Solid Electrolyte Interphase Evolution on Lithium Metal Electrodes Followed by Scanning Electrochemical Microscopy Under Realistic Battery Cycling Current Densities. *ChemElectroChem*, 2020, **7**, 3590-3596.

64   Z. T. Gossage, J. Hui, Y. Zeng, H. Flores-Zuleta and J. Rodriguez-Lopez. Probing the reversibility and kinetics of Li(+) during SEI formation and (de)intercalation on edge plane graphite using ion-sensitive scanning electrochemical microscopy. *Chem. Sci.*, 2019, **10**, 10749-10754.

65   J. Hui, M. Burgess, J. Zhang and J. Rodriguez-Lopez. Layer Number Dependence of Li(+) Intercalation on Few-Layer Graphene and Electrochemical Imaging of Its Solid-Electrolyte Interphase Evolution. *ACS Nano*, 2016, **10**, 4248-4257.

66   G. Zampardi, E. Ventosa, F. La Mantia and W. Schuhmann. Scanning Electrochemical Microscopy Applied to the Investigation of Lithium (De-)Insertion in TiO2. *Electroanalysis*, 2015, **27**, 1017-1025.

67   H. Bulter, F. Peters, J. Schwenzel and G. Wittstock. Investigation of Electron Transfer Properties of the SEI on Metallic Lithium Electrodes by SECM at Open Circuit. *ECS Transactions*, 2015, **66**, 69-79.

68   D. Bar-Tow. A Study of Highly Oriented Pyrolytic Graphite as a Model for the Graphite Anode in Li-Ion Batteries. *J. Electrochem. Soc.*, 1999, **146**, 824.

69   K. Xu and A. von Wald Cresce. Li+-solvation/desolvation dictates interphasial processes on graphitic anode in Li ion cells. *J. Mater. Res.*, 2012, **27**, 2327-2341.

70   R. J. Rice and R. L. McCreery. Quantitative Relationship between Electron Transfer Rate and Surface Microstructure of Laser-Modified Graphite Electrodes. *Anal. Chem.*, 1989, **61**, 1637-1641.

71   Y. Domi, M. Ochida, S. Tsubouchi, H. Nakagawa, T. Yamanaka, T. Doi, T. Abe and Z. Ogumi. In Situ AFM Study of Surface Film Formation on the Edge Plane of HOPG for Lithium-Ion Batteries. *The Journal of Physical Chemistry C*, 2011, **115**, 25484-25489.

72   D. Martín-Yerga, M. Kang and P. R. Unwin. Scanning Electrochemical Cell Microscopy in a Glovebox: Structure-Activity Correlations in the Early Stages of Solid-Electrolyte Interphase Formation on Graphite. *ChemElectroChem*, 2021, **8**, 4240-4251.

73   L. Seidl, S. Martens, J. Ma, U. Stimming and O. Schneider. In situ scanning tunneling microscopy studies of the SEI formation on graphite electrodes for Li(+)-ion batteries. *Nanoscale*, 2016, **8**, 14004-14014.

74   H. Bülter, F. Peters, J. Schwenzel and G. Wittstock. Comparison of Electron Transfer Properties of the SEI on Graphite Composite and Metallic Lithium Electrodes by SECM at OCP. *J. Electrochem. Soc.*, 2015, **162**, A7024-A7036.

75   X. Zeng, D. Liu, S. Wang, S. Liu, X. Cai, L. Zhang, R. Zhao, B. Li and F. Kang. In Situ Observation of Interface Evolution on a Graphite Anode by Scanning Electrochemical Microscopy. *ACS Appl. Mater. Interfaces*, 2020, **12**, 37047-37053.

76   E. Ventosa, B. Mei, W. Xia, M. Muhler and W. Schuhmann. TiO2 (B)/anatase composites synthesized by spray drying as high performance negative electrode material in li-ion batteries. *ChemSusChem*, 2013, **6**, 1312-1315.

77   E. Madej, F. La Mantia, B. Mei, S. Klink, M. Muhler, W. Schuhmann and E. Ventosa. Reliable benchmark material for anatase TiO2 in Li-ion batteries: On the role of dehydration of commercial TiO2. *J. Power Sources*, 2014, **266**, 155-161.

78   M. Zukalová, M. Kalbáč, L. Kavan, I. Exnar and M. Graetzel. Pseudocapacitive Lithium Storage in TiO2(B). *Chem. Mater.*, 2005, **17**, 1248-1255.

79   A. R. Armstrong, G. Armstrong, J. Canales, R. García and P. G. Bruce. Lithium-Ion Intercalation into TiO2-B Nanowires. *Adv. Mater.*, 2005, **17**, 862-865.

80   E. Ventosa, E. Madej, G. Zampardi, B. Mei, P. Weide, H. Antoni, F. La Mantia, M. Muhler and W. Schuhmann. Solid Electrolyte Interphase (SEI) at TiO2 Electrodes in Li-Ion Batteries: Defining Apparent and Effective SEI Based on Evidence from X-ray Photoemission Spectroscopy and Scanning Electrochemical Microscopy. *ACS Appl. Mater. Interfaces*, 2017, **9**, 3123-3130.

81   W. An, B. Gao, S. Mei, B. Xiang, J. Fu, L. Wang, Q. Zhang, P. K. Chu and K. Huo. Scalable synthesis of ant-nest-like bulk porous silicon for high-performance lithium-ion battery anodes. *Nat. Commun.*, 2019, **10**, 1-11.

82   D. Ma, Z. Cao and A. Hu. Si-Based Anode Materials for Li-Ion Batteries: A Mini Review. *Nano-Micro Lett.*, 2014, **6**, 347-358.

83   M. N. Obrovac and L. Christensen. Structural Changes in Silicon Anodes during Lithium Insertion/Extraction. *Electrochem. Solid-State Lett.*, 2004, **7**, A93.

84   M. Sternad, M. Forster and M. Wilkening. The microstructure matters: Breaking down the barriers with single crystalline silicon as negative electrode in Li-ion batteries. *Sci. Rep.*, 2016, **6**, 1-8.

85   U. S. Vogl, S. F. Lux, E. J. Crumlin, Z. Liu, L. Terborg, M. Winter and R. Kostecki. The Mechanism of SEI Formation on a Single Crystal Si(100) Electrode. *J. Electrochem. Soc.*, 2015, **162**, A603.

86   E. dos Santos Sardinha, M. Sternad, H. M. R. Wilkening and G. Wittstock. Nascent SEI-Surface Films on Single Crystalline Silicon Investigated by Scanning Electrochemical Microscopy. *ACS Appl. Energy Mater.*, 2019, **2**, 1388-1392.

87   K. Mizushima, P. C. Jones, P. J. Wiseman and J. B. Goodenough. $LixCoO_2$ (0<x<-1): A new cathode material for batteries of high energy density. *Mater. Res. Bull.*, 1980, **15**, 783-789.

88   S. Kalluri, M. Yoon, M. Jo, S. Park, S. Myeong, J. Kim, S. X. Dou, Z. Guo and J. Cho. Surface Engineering Strategies of Layered LiCoO2Cathode Material to Realize High-Energy and High-Voltage Li-Ion Cells. *Adv. Energy Mater.*, 2017, **7**, 1601507.

89   T. Fang, J. G. Duh and S. R. Sheen. Improving the Electrochemical Performance of LiCoO2 Cathode by Nanocrystalline ZnO Coating. *J. Electrochem. Soc.*, 2005, **152**, A1701-A1706.

90   Y. J. Kim, J. Cho, T.-J. Kim and B. Park. Suppression of Cobalt Dissolution from the LiCoO2 Cathodes with Various Metal-Oxide Coatings. *J. Electrochem. Soc.*, 2003, **150**, A1723-A1725.

91   H. Wang, Y. I. Jang, B. Huang, D. R. Sadoway and Y. M. Chiang. TEM Study of Electrochemical Cycling-Induced Damage and Disorder in LiCoO2 Cathodes for Rechargeable Lithium Batteries. *J. Electrochem. Soc.*, 1999, **146**, 473-480.

92   J. Cho, Y. J. Kim and B. Park. LiCoO2 Cathode Material That Does Not Show a Phase Transition from Hexagonal to Monoclinic Phase. *J. Electrochem. Soc.*, 2001, **148**, A1110-A1115.

93   B. Michalak, H. Sommer, D. Mannes, A. Kaestner, T. Brezesinski and J. Janek. Gas Evolution in Operating Lithium-Ion Batteries Studied In Situ by Neutron Imaging. *Sci. Rep.*, 2015, **5**, 1-9.

94   G. A. Snook, T. D. Huynh, A. F. Hollenkamp and A. S. Best. Rapid SECM probing of dissolution of LiCoO2 battery materials in an ionic liquid. *J. Electroanal. Chem.*, 2012, **687**, 30-34.

95   J. Lu, C. Zhan, T. Wu, J. Wen, Y. Lei, A. J. Kropf, H. Wu, D. J. Miller, J. W. Elam, Y. K. Sun, X. Qiu and K. Amine. Effectively suppressing dissolution of manganese from spinel lithium manganate via a nanoscale surface-doping approach. *Nat. Commun.*, 2014, **5**, 1-8.

96   C. Zhan, J. Lu, A. Jeremy Kropf, T. Wu, A. N. Jansen, Y. K. Sun, X. Qiu and K. Amine. Mn(II) deposition on anodes and its effects on capacity fade in spinel lithium manganate-carbon systems. *Nat. Commun.*, 2013, **4**, 1-8.

97   S. Komaba, N. Kumagai and Y. Kataoka. Influence of manganese(II), cobalt(II), and nickel(II) additives in electrolyte on performance of graphite anode for lithium-ion batteries. *Electrochim. Acta*, 2002, **47**, 1229-1239.

98   A. Mishra, D. Sarbapalli, M. S. Hossain, Z. T. Gossage, Z. Li, A. Urban and J. Rodríguez-López. Highly Sensitive Detection and Mapping of Incipient and Steady-State Oxygen Evolution from Operating Li-Ion Battery Cathodes via Scanning Electrochemical Microscopy. *J. Electrochem. Soc.*, 2022, **169**, 086501.

99   M. E. Snowden, A. G. Guell, S. C. Lai, K. McKelvey, N. Ebejer, M. A. O'Connell, A. W. Colburn and P. R. Unwin. Scanning electrochemical cell microscopy: theory and experiment for quantitative high resolution spatially-resolved voltammetry and simultaneous ion-conductance measurements. *Anal. Chem.*, 2012, **84**, 2483-2491.

100   A. Kumatani, Y. Takahashi, C. Miura, H. Ida, H. Inomata, H. Shiku, H. Munakata, K. Kanamura and T. Matsue. Scanning electrochemical cell microscopy for visualization and local electrochemical activities of lithium-ion (de) intercalation process in lithium-ion batteries electrodes. *Surf. Interface. Anal.*, 2019, **51**, 27-30.

101   S. R. Catarelli, D. Lonsdale, L. Cheng, J. Syzdek and M. Doeff. Intermittent Contact Alternating Current Scanning Electrochemical Microscopy: A Method for Mapping Conductivities in Solid Li Ion Conducting Electrolyte Samples. *Front. Energy Res.*, 2016, **4**, 14.

102   Y. Takahashi, T. Yamashita, D. Takamatsu, A. Kumatani and T. Fukuma. Nanoscale kinetic imaging of lithium ion secondary battery materials using scanning electrochemical cell microscopy. *Chem. Commun.*, 2020, **56**, 9324-9327.

103   H. Bülter, F. Peters, J. Schwenzel and G. Wittstock. In Situ Quantification of the Swelling of Graphite Composite Electrodes by Scanning Electrochemical Microscopy. *J. Electrochem. Soc.*, 2015, **163**, A27-A34.

104   N. Ebejer, A. G. Guell, S. C. Lai, K. McKelvey, M. E. Snowden and P. R. Unwin. Scanning electrochemical cell microscopy: a versatile technique for nanoscale electrochemistry and functional imaging. *Annu. Rev. Anal. Chem.*, 2013, **6**, 329-351.

105   K. Eckhard and W. Schuhmann. Alternating current techniques in scanning electrochemical microscopy (AC-SECM). *Analyst*, 2008, **133**, 1486-1497.

106   M. Etienne, A. Schulte and W. Schuhmann. High resolution constant-distance mode alternating current scanning electrochemical microscopy (AC-SECM). *Electrochem. Commun.*, 2004, **6**, 288-293.

107   D. Trinh, M. Keddam, X. R. Novoa and V. Vivier. Alternating current measurements in scanning electrochemical microscopy, part 2: detection of adsorbates. *Chemphyschem*, 2011, **12**, 2177-2183.

108   D. Liu, X. Zeng, S. Liu, S. Wang, F. Kang and B. Li. Application of Alternating Current Scanning Electrochemical Microscopy in Lithium-Ion Batteries: Local Visualization of the Electrode Surface. *ChemElectroChem*, 2019, **6**, 4854-4858.

109   K. R. Tallman, S. Yan, C. D. Quilty, A. Abraham, A. H. McCarthy, A. C. Marschilok, K. J. Takeuchi, E. S. Takeuchi and D. C. Bock. Improved Capacity Retention of Lithium Ion Batteries under Fast Charge via Metal-Coated Graphite Electrodes. *J. Electrochem. Soc.*, 2020, **167**.

110   M. S. Hossain, L. I. Stephens, M. Hatami, M. Ghavidel, D. Chhin, J. I. G. Dawkins, L. Savignac, J. Mauzeroll and S. B. Schougaard. Effective Mass Transport Properties in Lithium Battery Electrodes. *ACS Appl. Energy Mater.*, 2019, **3**, 440-446.

111   J. Menzel, A. Slesinski, P. Galek, P. Bujewska, A. Kachmar, E. Frąckowiak, A. Washio, H. Yamamoto, M. Ishikawa and K. Fic. Operando monitoring of activated carbon electrodes operating with aqueous electrolytes. *Energy Storage Mater.*, 2022, **49**, 518-528.

112   S.-K. Jeong, M. Inaba, R. Mogi, Y. Iriyama, T. Abe and Z. Ogumi. Surface Film Formation on a Graphite Negative Electrode in Lithium-Ion Batteries: Atomic Force Microscopy Study on the Effects of Film-Forming Additives in Propylene Carbonate Solutions. *Langmuir*, 2001, **17**, 8281-8286.

113   X. Shi, W. Qing, T. Marhaba and W. Zhang. Atomic force microscopy - Scanning electrochemical microscopy (AFM-SECM) for nanoscale topographical and electrochemical characterization: Principles, applications and perspectives. *Electrochim. Acta*, 2020, **332**, 135472.

114   G. Zampardi, S. Klink, V. Kuznetsov, T. Erichsen, A. Maljusch, F. La Mantia, W. Schuhmann and E. Ventosa. Combined AFM/SECM Investigation of the Solid Electrolyte Interphase in Li-Ion Batteries. *ChemElectroChem*, 2015, **2**, 1607-1611.

115   M. Etienne, M. Dossot, J. Grausem and G. Herzog. Combined Raman microspectrometer and shearforce regulated SECM for corrosion and self-healing analysis. *Anal. Chem.*, 2014, **86**, 11203-11210.

116   S. Ackermann, M. Steimecke, C. Morig, U. Spohn and M. Bron. A complementary Raman and SECM study on electrically conductive coatings based on graphite sol-gel composite electrodes for the electrochemical antifouling. *J. Electroanal. Chem.*, 2017, **795**, 68-74.

117   J. Clausmeyer, M. Nebel, S. Grutzke, Y. U. Kayran and W. Schuhmann. Local Surface Modifications Investigated by Combining Scanning Electrochemical Microscopy and Surface-Enhanced Raman Scattering. *Chempluschem*, 2018, **83**, 414-417.

118   N. B. Schorr, A. Jiang and J. Rodriguez-Lopez. Probing Graphene Interfacial Reactivity via Simultaneous and Colocalized Raman-Scanning Electrochemical Microscopy Imaging and Interrogation. *Anal. Chem.*, 2018, **90**, 7848-7854.

119   M. Steimecke, G. Seiffarth and M. Bron. In Situ Characterization of Ni and Ni/Fe Thin Film Electrodes for Oxygen Evolution in Alkaline Media by a Raman-Coupled Scanning Electrochemical Microscope Setup. *Anal. Chem.*, 2017, **89**, 10679-10686.

120   L. Wang, J. Kowalik, B. Mizaikoff and C. Kranz. Combining Scanning Electrochemical Microscopy with Infrared Attenuated Total Reflection Spectroscopy for in Situ Studies of Electrochemically Induced Processes. *Anal. chem.*, 2010, **82**, 3139-3145.

121   A. E. Dorfi, H. W. Kuo, V. Smirnova, J. Wright and D. V. Esposito. Design and operation of a scanning electrochemical microscope for imaging with continuous line probes. *Rev. Sci. Instrum.*, 2019, **90**, 083702.

122   Y. Leroux, D. Schaming, L. Ruhlmann and P. Hapiot. SECM Investigations of Immobilized Porphyrins Films. *Langmuir*, 2010, **26**, 14983-14989.

123   E. Garcia-Quismondo, S. Alvarez-Conde, G. Garcia, J. I. Medina-Santos, J. Palma and E. Ventosa. New Technique for Probing the Protecting Character of the Solid Electrolyte Interphase

as a Critical but Elusive Property for Pursuing Long Cycle Life Lithium-Ion Batteries. *ACS Appl. Mater. Interfaces*, 2022, **14**, 43319-43327.

124   S. Liu, D. Liu, S. Wang, X. Cai, K. Qian, F. Kang and B. Li. Understanding the cathode electrolyte interface formation in aqueous electrolyte by scanning electrochemical microscopy. *J. Mater. Chem. A*, 2019, **7**, 12993-12996.